Photodissociation at 193 nm of *tert*-Butyl Nitrite on Ag(111)†

W. Zhao,‡ I. Lee,§ S. K. Kim,§ and J. M. White*,‡

Department of Chemistry & Biochemistry, University of Texas at Austin, Austin, Texas 78712-1167, and Department of Chemistry, Sungkyunkwan University, Suwon 440-746, South Korea

Received: January 13, 2004

The translational and internal state properties of nitric oxide, NO, ejected by 193-nm photodissociation of *tert*-butyl nitrite, $(CH_3)_3CONO$, TBN, adsorbed on Ag(111) have been investigated using resonance-enhanced multiphoton ionization time-of-flight (REMPI-TOF) and quadrupole mass spectrometer time-of-flight (QMS-TOF). The results are described in terms of three components depending on the number of collisions along the exit trajectory and are compared to prior work using 248- and 351-nm photons. Although 193-nm photons have higher energy, the characteristic translational energy of the collisionless NO (0.55 eV) lies between that for 248 nm (0.89 eV) and 351 nm (0.39 eV). As for gas-phase photolysis at 193 nm, the NO is rotationally cold ($J_{max} = 15.5$), much lower than for both 248- ($J_{max} = 53.5$) and 351-nm ($J_{max} = 31.5$) photolysis. The NO vibrational distribution is dominated by $v'' = 1$, whereas $v'' = 0$ for 248 nm and $v'' = 1$ and 2 for 351 nm photodissociations, respectively. Angle-resolved REMPI-TOF and QMS-TOF studies give information about the orientation of adsorbed TBN. While TBN is more stable with the C−O−N═O plane perpendicular to surface and the internal O−N bond directed about 40° away from the surface normal, dosing less than a full monolayer at 80 K does not achieve this state fully. Annealing to 110 K is sufficient to realize this molecular orientation. For multilayer coverage dosed at 80 K, the data are consistent with considerable surface roughness compared to a surface annealed at 110 K.

1. Introduction

Surface photochemistry has been of interest for many years.[1−3] Among the motivations are its many potential technological applications, e.g., photochemical lithography, deposition, and etching related to the fabrication of electronic and chemical sensor devices with submicron dimensions. There also continues to be scientific interest in fundamental questions concerning the mechanisms of energy transfer among the radiation field, and the various electronic and nuclear degrees of freedom of adsorbate−substrate systems.

The spectroscopy and photodissociation dynamics of aliphatic nitrites (R−O−N═O) have been the subject of much interest.[4−9] Typically, gas phase and adsorbed nitrites dissociate upon photolysis and do so through cleavage of the internal O−N bond to from an alkoxide and nitric oxide. Like other nitrites, *tert*-butyl nitrite (TBN, $(CH_3)_3CONO$) has three distinct optical absorption bands, the lowest energy band is found between 300 and 400 nm ($n \rightarrow \pi^*$, $S_1 \leftarrow S_0$), and motion on S_1 is characterized as vibrational predissociation. The second band ranges from about 216 to 280 nm ($\pi \rightarrow \pi^*$, $S_2 \leftarrow S_0$), and motion on S_2 is described as a very fast repulsive dissociation. The third band, rarely studied and related to this paper, ranges from 180 to 216 nm and also leads to dissociation of the internal O−N bond. State-resolved studies of NO reveal very different quantum state distributions depending on the photolysis wavelength. For gas-phase irradiation, photodissociation at 351 nm results in vibrationally hot, rotationally and translationally cold NO molecules, photodissociation at 248 nm produces vibrationally cold but rotationally and translationally hot NO molecules, and photodissociation at 193 nm produces NO with less average translational and rotational energy than when 248-nm photons are used.[8,10−14] Thus, even though the photon energy is 1.5 eV higher at 193 nm than at 248 nm, much less of the available energy is transferred to NO. When adsorbed, adsorbate−adsorbate and adsorbate−substrate interactions do not significantly alter the dissociation of alkyl nitrites but do alter the subsequent dynamics and thereby alter the internal and translational energy distributions.[15−25]

To complement previous studies,[22−25] in this paper we extend the excitation wavelength to 193 nm. Both resonance-enhanced multiphoton ionization time-of-flight (REMPI-TOF) and quadrupole mass spectrometer time-of-flight (QMS-TOF) tools were employed to study the NO dynamics produced by TBN photodissociation. As in earlier reports, the recorded intensity vs time data were represented in terms of trimodal distributions of NO. An angle-resolved study provides information about the orientation of adsorbed TBN molecules and how the orientation is altered by thermal annealing.

2. Experimental Section

2.1. Apparatus. The experimental apparatus has been described elsewhere.[22−25] Concisely, the experiments were done in a two-level ultrahigh vacuum (UHV) chamber operated at a base pressure of 8×10^{-11} Torr that was pumped by a 360 L/s turbomolecular pump and a 6-in. diameter diffusion pump. The upper level includes an ion gun for cleaning the substrate, doser for supplying TBN, reverse-view low-energy electron diffraction optics (LEED), and an Auger electron spectrometer for checking the sample cleanliness. The lower level includes an ion detector for gathering REMPI-TOF spectra (see below) and a rotatable, differentially pumped quadrupole mass spectrometer (QMS) for angle-resolved QMS-TOF measurements. The ionizing electron beam of the latter was located 12.5 cm from the silver surface.

Standard substrate-cleaning procedures were followed.[22] The Ag substrate can be cooled to 80 K from 800 K in less than 15 min by contact with a liquid nitrogen reservoir. Heating was accomplished resistively and was limited to 850 K to avoid evaporating Ag. The *tert*-butyl nitrite (TBN) (Aldrich, 90%) was freeze−pump−thawed a few times before introduction into

† Part of the special issue "Gerhard Ertl Festschrift".

* To whom correspondence may be addressed. E-mail: jmwhite@mail.utexas.edu.

‡ University of Texas.

§ Sungkyunkwan University.

10.1021/jp049829g CCC: $27.50
Published on Web 04/09/2004

the UHV chamber. Dosing was performed through a valve connected to a tiny pinhole (~60 μm diameter), and then to a 3-mm ID tube directed at the Ag(111) surface. The pinhole is located ~1 in. from the substrate, to ensure uniform dosage. The chamber pressure rose to 2×10^{-9} Torr during dosing and returned to the initial vacuum level promptly upon closing the doser valve.

In previous work,[26] we have shown that TPD spectra as a function of TBN coverage show a multilayer contribution before the monolayer is fully saturated. In this paper, we define a standard dose (1 SD) as the highest dose at 80 K for which there is no contribution from the multilayer peak in subsequent TPD. The corresponding TBN TPD peak area is 65% of that corresponding to a fully saturated monolayer, i.e., 1 SD = 0.65 ML. To prepare a saturated monolayer at 80 K in the absence of a multilayer was accomplished by dosing more than 3.5 SD at 80 K, heating at 0.5 K/s to 140 K, and promptly recooling to 80 K.

Adsorbed TBN was photolyzed using an excimer laser operating at 193 nm. To reduce the laser output below the 0.1 mJ/cm^2, the output pulses were attenuated with a metal mesh and several neutral density filters. No more than 10% of the initial TBN coverage was photodissociated in a typical REMPI-TOF (~2000 pulses) or QMS-TOF (~4000 pulses) experiment.

The desorbing NO was characterized using a two-photon (1 + 1) REMPI-TOF scheme. The fundamental wavelength (1064 nm) of a Nd:YAG laser was tripled to 355 nm to pump the dye laser. Coumarin 2 and 102 dye solutions were used for examining NO vibrational states $v'' = 0$, and for $v'' = 1$ and 2, respectively. The output of the dye laser was doubled using a BBO−B crystal, and the dye laser fundamental output was rejected using a harmonic separator. For data taken along the surface normal, the REMPI laser beam (~1 mJ/pulse, 12 ns) traveled parallel to the substrate surface and was focused by a cylindrical lens at a distance of 3.5 cm from the plane of the surface. The NO^+, created by firing the REMPI laser at selected delay times after the excimer laser pulse, was detected using a Wiley−McLaren-type time-of-flight device outfitted with a microchannel plate (MCP) detector. The ion signal was gated, read into a boxcar integrator, and output to a computer interface. A digital delay/pulse generator controlled the time delay between the photolysis and probe lasers. The intensities of both the excimer and REMPI lasers were monitored by photodiodes, and their signals were used to normalize the measured NO^+ intensities. The NO REMPI-TOF spectra were collected with the detector located at two angles, 0 and 35° with respect to the surface normal of Ag(111). For data collected at 35°, the REMPI laser beam was not parallel to the Ag(111) surface. The laboratory direction of the sample normal was rotated 35°, whereas the REMPI laser direction was not changed.

In some experiments, the NO was detected without state resolution using a QMS-TOF scheme that averaged the results of 4,000 laser pulses with a multichannel scaler (0.640 μs resolution). Angle-resolved TOF spectra were taken by rotating the QMS around the sample (in the plane defined by incident and reflected He−Ne laser beam used to align the system). To check for electron-induced dissociation, we monitored TPD spectra taken at various delay times and found no measurable dissociation in 10 min. Each QMS-TOF photolysis experiment took about 7 min.

2.2. Data Fitting. The analysis of TOF spectra was detailed in our previous papers.[22−25] We revisited the fitting protocols used to account for three different categories of relaxation—unrelaxed, partially thermalized, and thermalized to the substrate temperature—and included a component to account for the pumping characteristics of our system.

Denoted as the *collisionless component*, unrelaxed high-velocity NO molecules arise from the surface by photodissociation of TBN no collisions before ejection into vacuum. The distribution can be described by Gaussian function

$$Y_{\text{collisionless}} = a_0 \exp\left\{-\frac{1}{2}\left(\frac{t-a_1}{a_2}\right)^2\right\} \quad (1)$$

where t is the time, a_0 is the amplitude, a_1 is the center of the Gaussian function, and a_2, the Gaussian standard deviation, controls the width of $Y_{\text{collisionless}}$. In practice, the collisionless component fitting involved a least-squares fit with the constraint that the final result provided an excellent fit to the leading edge of TOF spectra.

The fully thermalized component assumes multiple collisions along the exit trajectory to form a physisorbed state of NO from which there is slow thermal desorption governed by the substrate temperature. A Maxwell−Boltzmann (MB) distribution was used to describe this component

$$Y_{\text{thermal}} = b_0 T^{-3/2} t^{-4} \exp\left\{-\frac{m}{2kT}\left(\frac{b_1}{t}\right)^2\right\} \quad (2)$$

where t is the time, T is the temperature, b_0 is the amplitude, b_1 is the fight distance, m is the mass of an NO molecule, and k is Boltzmann's constant.

Under our conditions, the MB distribution does not account fully for the intensity at very long times, i.e., longer than twice the position of the MB maximum. This excess is ascribed to limited effective pumping speed and is accounted for using the exponentially decaying function

$$Y_{\text{pumptail}} = c_0 \exp\left\{-\frac{(t-c_1)}{c_2}\right\} \quad \text{for} \quad t > c_1$$
$$= 0 \quad \text{for} \quad t \le c_1 \quad (3)$$

where t is the time, c_0 is the amplitude, c_2 is the pumping time constant, and c_1 is the time where a given QMS-TOF or REMPI-TOF profiles reaches its maximum value, i.e., where the local pressure maximizes. In passing, it is noteworthy that a single value of c_2 adequately described the long tail in all our QMS-TOF and REMPI-TOF data.

If we subtract the above distributions from the total TOF intensity (Y_{total}), e.g., $Y_{\text{total}} - Y_{\text{collisonless}} - Y_{\text{thermal}} - Y_{\text{pumptail}}$, there is residual intensity positioned between the Gaussian and the MB components. This is ascribed to partially thermalized NO, i.e., trajectories involving one or a few collisions that leave the exiting NO with partial memory of its nascent condition. This portion of NO can be described by one or more modified Maxwell−Boltzmann (MBB) distributions

$$Y_{\text{intermediate}} = \frac{d_0}{t^4} \exp\left\{-\frac{m}{2kT}\left[\frac{d_1}{t} - d_2\right]^2\right\} \quad (4)$$

where t is the time, T is the temperature, d_0 is the amplitude, d_1 the flight distance, and d_2 is the velocity offset. While the full set of our data was not adequately described by a single MBB function, two MMBs were quite adequate. This is not unreasonable since the intermediate component should account for a wide variety of partially thermalized NO trajectories.

The final TOF data fitting equation is following as

$$Y_{\text{total}} = Y_{\text{collisionless}} + Y_{\text{intermediate}}(1) + Y_{\text{intermediate}}(2) + Y_{\text{thermal}} + Y_{\text{pumptail}} \quad (5)$$

The fitting of eq 5 to the data was performed by author-written computer code based on a nonlinear least-squares routine that provided standard error estimates to associate with the fitting parameters. The set of parameters for each of the functions in eq 5 were acquired by fitting three intense REMPI spectra. The resulting values, with only minor adjustments, provided adequate fits for all the other REMPI-TOF and QMS-TOF spectra. Operationally, the time scale of the REMPI data was multiplied by 3.57 to account for the different flight distances involved −3.5 cm for REMPI-TOF and 12.5 cm for QMS-TOF.

Since both REMPI and QMS spectra are taken with density detectors, the fitting distributions are in flux-weighted form, i.e., the number of molecules arriving per unit time. A measure of the number of the molecules at each distribution can be obtained by integrating each flux-weighted form over time. The data are presented in the same units, albeit arbitrary. To simplify the data presentation, the figures show the collisionless, intermediate, and thermal components; the pumping tail was subtracted and is not shown.

3. Results

TBN TPD has been presented in our previous paper.[26] The monolayer desorbs from Ag(111) at 160 K and the multilayer at 130 K. As noted earlier, the multilayer peak appears before the monolayer saturates. For 1 SD, the coverage is 0.65 monolayer (ML), so 40 SD is enough TBN to form 26 ML. This must be taken as an effective coverage since as-dosed TBN evidences 3D island, not layer-by-layer, growth. To prepare a 1-ML TBN, more than 3.5 SD must be dosed, and the substrate annealed to 140 K to desorb the multilayer. Annealing from 80 to 110 K desorbs no TBN but does, as we illustrate below, alter its structure.

3.1. Internal State Distributions for a Thick Multilayer. Figure 1 summarizes a state-resolved study of NO produced by 193-nm photodissociation of 40 SD TBN held at 110 K on Ag(111). The REMPI-TOF detector was aligned along the surface normal. The upper panel shows spectra for $v'' = 0$ and $J = 5.5$, 15.5, and 20.5, whereas the lower panel shows analogous data for $v'' = 1$. For each case, the experimental points are shown as circles, the individual components as thin lines, and their sum as a thick line. The integrated areas of the three components are summarized in the inserted tables. It is noteworthy that, for $v'' = 0$ (Figure 1a), both the $J = 5.5$ and 15.5 spectra required contributions from all three components, while the $J = 20.5$ spectrum was fit adequately with no thermalized component. For $v'' = 1$ (Figure 1b), the $J = 15.5$ and 20.5 spectra were also fit adequately with no thermalized component but the $J = 5.5$ spectrum required a small thermalized contribution. For the collisionless components of both $v'' = 0$ and 1, the $J = 15.5$ state carries the most intensity. For the translationally thermalized component, on the other hand, the $J = 5.5$ intensity carries the most intensity. While there is some intensity at J values higher than 20.5, the signal-to-noise ratio was too low to allow reasonable fitting.

3.2. Effect of Annealing Submonolayer and Multilayer Coverages. To probe the coverage-dependent and angle-dependent properties of the REMPI spectra, the $v'' = 1$ and $J = 15.5$ state was selected since this state is most intense in Figure 1. For 1 SD doses at 80 K, there was a strong angular and photolysis temperature dependence of the REMPI-TOF spectra (Figure 2). The lower and upper panels of Figure 2 show data gathered with the REMPI detector aligned along and 35° away from the surface normal, respectively. The lower and upper curves in each panel were gathered for 1 SD dosed at 80 K and photolyzed at 80 and 110 K, respectively. The integrated areas of the three components are summarized in the inserted tables. In summary, the total intensity (12.35 and 15.75) is higher for $v'' = 1$ and $J = 15.5$ NO ejected 35° away from the surface normal compared with NO ejected along the surface normal (3.53 and 8.72). Similarly, the collisionless component has a higher intensity at 35° (2.81 and 2.51) than at 0° (0.16 and 0.56). More interestingly, for the $v'' = 1$ and $J = 15.5$ NO ejected at 35°, the collisionless component was slightly higher at 110 K (2.81) than at 80 K (2.51). The opposite held at 0°, i.e., 0.16 at 110 K compared to 0.56 at 80 K. Interestingly, the translationally thermalized $v'' = 1$ and $J = 15.5$ NO component has much more intensity along the surface normal at 80 K (3.03) than at 110 K (0.80).

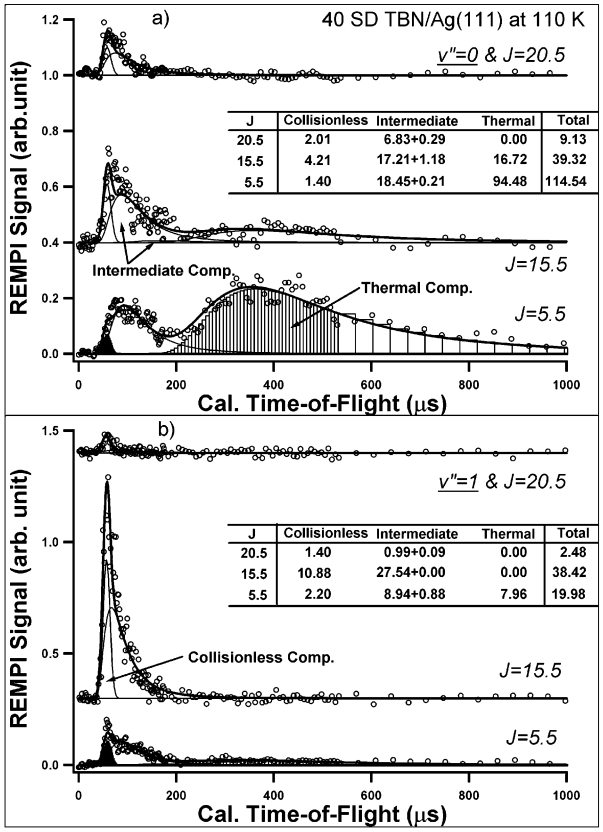

J	Collisionless	Intermediate	Thermal	Total
20.5	2.01	6.83+0.29	0.00	9.13
15.5	4.21	17.21+1.18	16.72	39.32
5.5	1.40	18.45+0.21	94.48	114.54

J	Collisionless	Intermediate	Thermal	Total
20.5	1.40	0.99+0.09	0.00	2.48
15.5	10.88	27.54+0.00	0.00	38.42
5.5	2.20	8.94+0.88	7.96	19.98

Figure 1. REMPI-TOF spectra of 40 SD TBN on Ag(111) at 110 K at the indicated combinations of J and v''. The thin solid lines are the fits, and the thick solid line is the summation of thin solid lines. The overlap of the data points (circles) is excellent. For the thermal component, a vertical line is used to indicate the fit at each data point. The integrated areas of the three components are summarized in the inserted table.

For comparison with the sub-monolayer dose of Figure 2 (0.65 ML), we dosed 40 SD at 80 K (26 ML equivalent) and tracked the $v'' = 1$, $J = 15.5$ REMPI-TOF spectra at 0° (lower panel) and 35° (upper panel) and at 80 and 110 K (Figure 3). For this dose, the total amount of ejected $v'' = 1$, $J = 15.5$ NO is about same at 0° (29.60) and 35° (28.86) for the as-dosed 80 K system but when warmed and photolyzed at 110 K, the analogous intensities are much higher along at 0° (38.07) than that at 35° (14.02). The thermal components are negligible in all four spectra, i.e., the sums of the collisionless and intermediate components are adequate. The intensity of the collisionless $v'' = 1$, $J = 15.5$ NO component ejected at 35° dropped from 6.01 to 2.61 for data gathered at 80 and 110 K, respectively. The reverse was found at 0° where the intensity of the collisionless $v'' = 1$, $J = 15.5$ NO rose from 2.51 to 10.53 for the 80 and 110 K data, respectively.

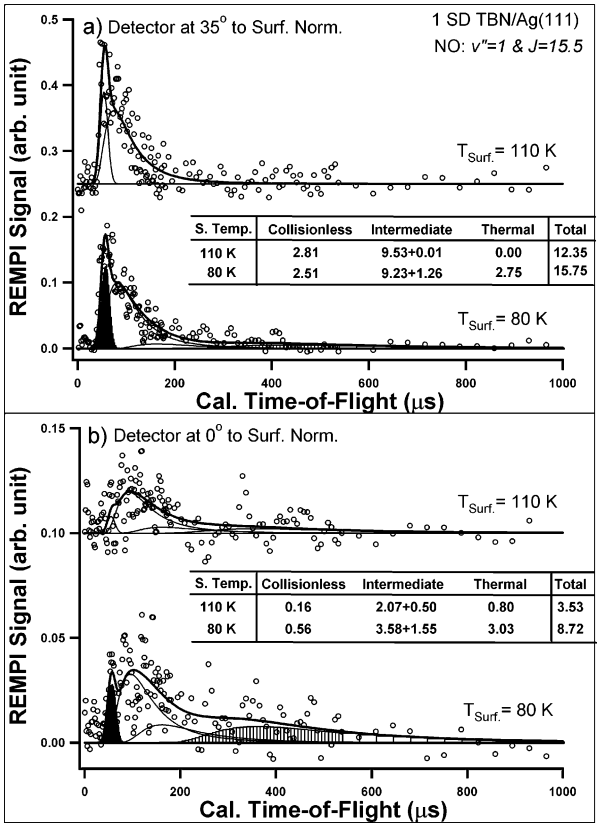

Figure 2. NO ($v'' = 1$ and $J = 15.5$) REMPI-TOF spectra of 1 SD TBN on Ag(111) at 80 and 110 K. The REMPI detector was aligned at 35 (a) and 0° (b) with respect to the surface normal. As in Figure 1, the thin solid lines are the fits, and the thick solid line is the summation of thin solid lines. The integrated areas of the three components are summarized in the inserted table.

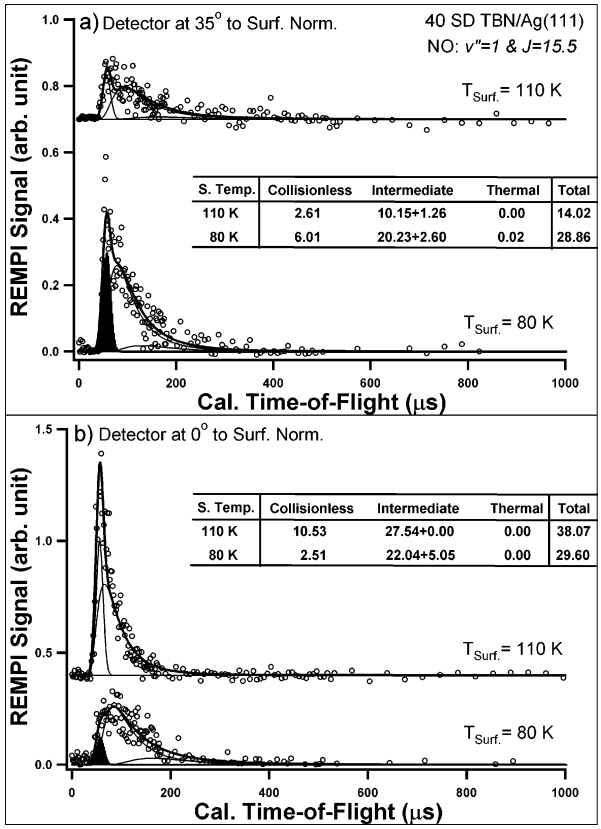

Figure 3. NO ($v'' = 1$ and $J = 15.5$) REMPI-TOF spectra of 40 SD TBN on Ag(111) at 80 and 110 K. The REMPI detector was aligned at 35 (a) and 0° (b) to surface normal. The thin solid lines are the fits, and the thick solid line is the summation of thin solid lines. The integrated areas of the three components are summarized in the inserted table.

3.3. Angle-Resolved, Not State-Resolved, TOF. A full angle- and state-resolved REMPI-TOF distribution is impractical for several reasons. Experimentally, it is impossible to rotate the substrate without changing the incident angle of the photolysis laser with respect to the substrate. In terms of time requirements, it is impractical to attempt to examine all the plausible (v'', J, angle) combinations. However, it is helpful to measure angular TOF distributions that are not state resolved by gathering QMS-TOF data for numerous detection angles (Figure 4). The TBN surface coverage was 1 ML, prepared as described above. The NO TOF data gathered at 40° away from the surface normal (upper panel) is fit very well with collisionless, two intermediate, and thermal components. The integrated intensities associated with the three types of NO are summarized in the lower panel for 11 angles ranging from 0 to 60°. Each of the three curves is normalized to unity at the maximum value. The collisionless component increased sharply (0.18 to 1.0) from 0 to 40° and then decreased sharply. The intermediate component rises and falls but not as sharply as the collisionless component. The intensity of the thermal component exhibits nearly constant intensity between 0 and 50° before, like the other two components, dropping sharply.

Table 1 lists the fitting parameters. With the exception of the temperature associated with the intermediate component, this set of parameters was used to describe all of the REMPI and QMS TOF data. The temperature of the intermediate component increased with the intensity of the collisionless component.

4. Discussion

4.1. 193-nm TBN Photodissociation Process. The gas-phase photodissociation of TBN at193 nm has been investigated with the following dissociation mechanism[10−11]

$$(CH_3)_3CONO + h\nu\ (193\ nm) \rightarrow (CH_3)_3CO\ (\tilde{A}) + NO\ (X^2\Pi)$$

i.e., the *t*-BuO radical, $(CH_3)_3CO$, is electronically excited. This implies that the dissociation dynamics is very different from studies[4−10] where longer-wavelength photons (above 216 nm) were used.

TBN photodissociation occurs on potential energy surfaces (PESs), which typically can be characterized by two coordinates R_{O-N} and $R_{N=O}$. The gas-phase S_2 PES is repulsive and monotonically decreases along the R_{O-N} coordinate; i.e., there is no barrier hindering immediate fragmentation once the molecule is photoexcited in the wavelength range between 216 and 300 nm. In this direct photodissociation, the coupling between R_{O-N} and $R_{N=O}$ coordinates is weak, and the exiting NO is ejected with little vibrational excitation, e.g., $v'' = 0$ is highly populated. Since R_{O-N} and $R_{N=O}$ are not linearly aligned, the angle between the two bond directions is about 100°, a large torque is applied to the N atom of the exiting NO molecule. This produces a very hot rotational distribution ($J_{max} = 53.5$ for $v'' = 0$). In contrast, the S_1 PES has a shallow minimum near the Franck−Condon transition region accessed when a photon is absorbed. As a result, the coupling between R_{O-N} and $R_{N=O}$ is stronger because vibrational excitation of the $R_{N=O}$ stretch influences the extension of R_{O-N}, the bond that breaks,

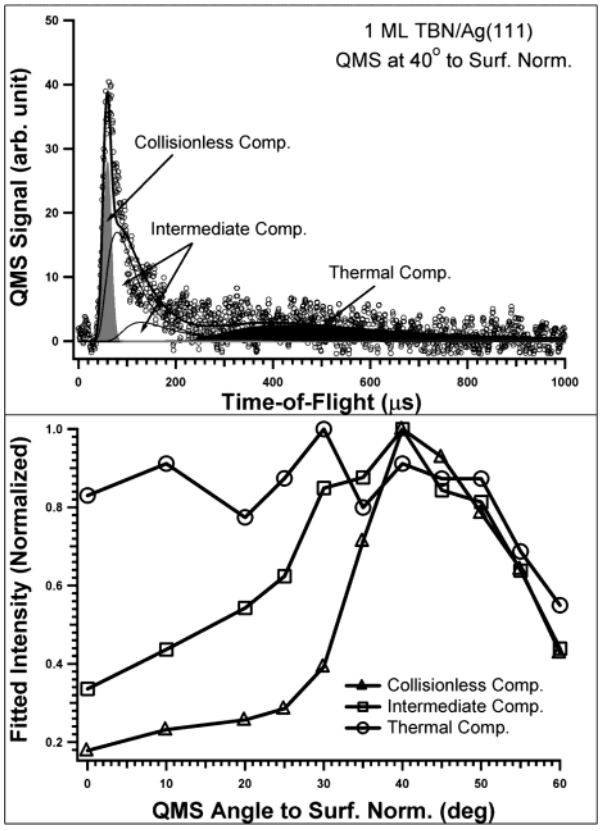

Figure 4. QMS-TOF spectra of 1 ML TBN photodissociation on Ag(111). (a) A typical example of data set and its fitting; (b) a summary of angle-resolved measurements. In part a, the solid gray region is the collisionless componenent, the black area is the fully thermalized component, and the white areas are the two MMB components. In part b, the intensities are normalized to unity at the maximum value of each component.

TABLE 1: Summary of the Data Fitting Parameters

parameter	value
Collisionless Component (Gaussian Distribution)	
Gaussian amplitude (a_0)	variable
center of Gaussian distribution (a_1)	55 ± 2 μs
Gaussian standard deviation (a_2)	8 ± 1 μs
Intermediate Component (Modified Maxwell−Boltzmann Distribution)	
First MMB	
MMB amplitude (d_0)	variable
NO flight distance (d_1)	REMPI, 3.5 cm; QMS, 12.5 cm
velocity offset (d_2)	40 m/s
MMB temperature (T)	1800 ± 180 K
Second MMB	
MMB amplitude (d_0)	variable
NO flight distance (d_1)	REMPI, 3.5 cm; QMS, 12.5 cm
velocity offset (d_2)	60 m/s
MMB temperature (T)	500 ± 50 K
Thermal Component (Maxwell−Boltzmann Distribution)	
MB amplitude (b_0)	variable
NO flight distance (b_1)	REMPI, 3.5 cm; QMS, 12.5 cm
MB temperature (T)	80 or 110 K
Pumping Tail (Exponential Decay)	
exponential amplitude (c_0)	variable
time to initiate the pumping tail (c_1)	50 ± 2 μs
exponential time constant (c_2)	7×10^{-4}

in the region of the shallow minimum, i.e., upon photon absorption, the path of steepest descent of the nascent TBN involves motion along the $R_{N=O}$ coordinate. Calculations predict that S_1-excited nitrite lives 5−10 vibrational periods of $R_{N=O}$ before R_{O-N} breaks.[2] Thus, the photodissociation of TBN through the S_1 PES is characterized as a vibrational predissociation and the ejected NO is vibrationally hotter (both $v'' = 1$ and 2 are populated), and rotationally less excited ($J_{max} = 31.5$) than excitation to S_2 (248 nm).

Compared to the gas phase, condensed or adsorbed TBN introduces additional coordinates. These account for the ground- and excited-state interactions between TBN and the substrate and TBN with other neighboring species to produce different translational and internal state distributions of NO. TBN surface photodissociation on Ag(111) by 248 and 351 nm was studied by our group previously.[22−25] The general conclusion is that the Ag substrate does not affect the dissociation mechanism but does influence subsequent dynamics. A trimodal (collisionless, intermediate, and thermal components) model was developed to interpret the observations. The translational and internal energy distributions of the collisionless component follow the gas phase while the intermediate and thermal components are attributed to collisional relaxation processes that occur along the trajectory of the ejected NO. In a similar analysis, bimodal distributions have been used to describe the photolysis of molecular clusters of TBN and TBN adsorbed on MgF_2.[15−21]

For 193-nm surface photodissociation, trimodal translational distributions adequately fit the spectra, the collisionless component tracks the gas-phase dissociation mechanism,[11] and the intermediate and thermal components display behaviors similar to those found for photolysis at 248 and 351 nm.[23−25] Although the photon energy is higher (6.5 compared to 5.0 eV), the characteristic translation energy of collisionless NO (0.55 eV) is lower than for 248 nm (0.89 eV). This result is consistent with the gas-phase photolysis result that the excitation at 193 nm occurs on a different electronic PES than at 248 nm. For 351-nm photolysis, the characteristic translational energy is lower (0.39 eV) than either that at 248 or at 193 nm. Moreover, the collisionless NO is rotationally colder ($J_{max} = 15.5$) at 193 nm than either 248- or 351-nm photodissociation. On the other hand, the vibrational excitation is mostly in $v'' = 1$ at 193 nm, $v'' = 0$ at 248 nm, and $v'' = 1$ and 2 at 351 nm.

In summary, a PES other than S_1 or S_2 is involved in the 193-nm photodissociation of TBN. This remains an open question for theoretical calculations.

4.2. TBN Surface Structure Model. In previous work, we have shown that TPD spectra as a function of TBN coverage show a multilayer contribution before the monolayer is fully saturated.[26] The results are modeled in terms of relatively strong intermolecular interactions that drive the formation of 3D islands before completion of the first layer. As a result, the adsorbate−vacuum interface of as-dosed multilayers at 80 K is rough on the length scale of the island diameters. The orientation of TBN molecules on Ag(111) has been examined by using reflection−absorption infrared spectroscopy (RAIRS).[19,26] For sub-monolayer coverages dosed at 80 K, strong N═O and N−O stretches were observed. This requires an average adsorption orientation with neither of these two bonds parallel to the Ag(111) surface.

For the multilayer, TBN desorption is negligible for annealing from 80 to 110 K, but there important changes in the RAIR spectra, i.e., peak narrowing and emergence of sidebands. The data indicate that annealing a multilayer from 80 to 110 K orders the whole film into monolayer and multilayer components that differ from each other but are each relatively homogeneous.[26]

The angle-resolved study of collisionless NO gives information about the orientation of the R_{O-N} coordinate in adsorbed TBN that lies at the adsorbate−vacuum interface. In Figure 2 (1 SD TBN on surface), the collisionless NO intensity at 35° (2.51) is 4.5 times stronger than that at 0° (0.56) for an as-deposited sub-monolayer (0.65 ML). Annealing to 110 K does not alter the coverage, but the 0° intensity decreases (0.16), while

the 35° intensity increases (2.81). Qualitatively, this agrees with RAIR results; annealing reorganizes adsorbed TBN molecules. For as-deposited TBN at 80 K, the most stable configuration is not realized, but annealing to 110 K provides enough thermal energy to generate the most stable structure on the time scale of a few minutes. In this configuration, TBN molecules align with the C_s plane (defined by the coplanar C−O−N═O region) nearly perpendicular to the surface and the average R_{O-N} bond coordinate is oriented about 40° away from the surface normal, consistent with the enhanced collilsionless intensity at 35° in the $v'' = 1$, $J = 15.5$ NO REMPI-TOF spectra.

For multilayer (40 SD in Figure 3), we suppose that the collisionless component arises only from those TBN molecules that are within the first layer at the adsorbate−vacuum interface. For the as-dosed multilayer, this first layer surface is quite rough and the layer is quite disordered. Consequently, the TBN molecules that contribute to the collisionless NO are not well-ordered with respect to the Ag(111) surface normal. The results obtained after annealing to 110 K indicate that this thermal energy does not desorb NO but does change the structure of the multilayer. By assumption that, consistent with the TPD results, a rather strong attractive intermolecular TBN-TBN interaction, annealing to 110 K would provide for increased local order with respect to neighboring molecules and, in addition, could lead to a smoother overall adsorbate−vacuum topology. To account for the increased collisionless NO intensity at 0° upon heating from 80 to 110 K, this model predicts that the reorientation and ordering favors moving the R_{O-N} coordinate toward the Ag(111) surface normal.

According to the proposed model, preparation of a saturated monolayer of TBN will form the most stable configuration since the as-dosed layer is thermally treated at 140 K. This should lead to a single layer with minimal local randomness and no long-range roughness. Consistent with this and an experimental report[22] and theoretical calculations,[28,29] the collisionless NO (Figure 4) exhibits a strong angular dependence favoring, by a factor of 7, ejection at 40° compared to 0°. The intermediate component follows a similar profile but increases by a factor of 3, indicating partial memory of its initial direction even after at one weak collision with the surroundings. The thermalized NO shows no significant angular dependence between 0 and 40°.

5. Summary

The surface photochemistry at 193 nm of *tert*-butyl nitrite on Ag(111) was investigated by REMPI-TOF and QMS-TOF for coverages of 1 SD, 40 SD, and 1 ML. A physically sensible trimodal collisional relaxation model, proposed in previous studies and modified slightly, was used to fit both REMPI-TOF and QMS-TOF data. The trimodal components are denoted as collisionless, intermediate, and thermal.

The collisionless component, described using a Gausssian distribution, had a characteristic translation energy of 0.55 eV, higher than for 351-nm (0.39 eV) but lower than for 248-nm (0.89 eV) photodissociation. The rotational state distribution of the collisionless component has a maximum near 15.5 for both $v'' = 0$ and 1. Similar results occur for monomolecular gas-phase photodissociation. Although the photon energy at 193 nm is 6.5 eV, the photodissociation appears to involve electronic states other than S_1 and S_2. The thermal translational energy component, described using a Maxwell−Boltzmann distribution, was consistent with fully thermalized NO molecules characterized by a temperature of 80 or 110 K and dominating the TOF spectrum at long times. The intermediate distribution accounts for all trajectories that have at least one weak collision but are not fully thermalized. This required one or two modified Maxwell−Boltzmann distributions for an adequate fit.

Angle-resolved REMPI-TOF and QMS-TOF data are consistent with average alignment of TBN with the C−O−N═O plane perpendicular to surface and the internal O−N bond directed about 40° away from the surface normal. For sub-monolayers dosed at 80 K, this state is not realized but can be reached by thermal annealing at 110 K. For multilayers dosed at 80 K, there is evidence for considerable surface roughness that can be reduced by annealing at 110 K.

Acknowledgment. Support by the National Science Foundation, Grant No. CHE00701122, and by the Robert A. Welch Foundation is gratefully acknowledged S.K.K is supported by the Korea Science and Engineering Foundation (Grant 98-0591-01-01-3).

References and Notes

(1) Ho, W. Surface Photochemistry. In *Laser Spectroscopy and Photochemistry on Metal Surfaces*; Dai, H.-L., Ho, W., Eds.; World Scientific: Singapore, 1995; Part II.
(2) Polanyi, J. C.; Zeiri, Y. Dynamics of Adsorbate Photochemistry. In *Laser Spectroscopy and Photochemistry on Metal Surfaces*; Dai, H.-L., Ho, W., Eds.; World Scientific: Singapore, 1995; Part II.
(3) Zhou, X. L.; White, J. M. Photodissociation and Photoreaction of Molecules Attached to Metal Surfaces. In *Laser Spectroscopy and Photochemistry on Metal Surfaces*; Dai, H.-L., Ho, W., Eds.; World Scientific: Singapore, 1995; Part II.
(4) Kades, E.; Rösslein, des. M.; Brühlmann, U.; Huber, J. R. *J. Phys. Chem.* **1993**, *97*, 989.
(5) *Molecular Photodissociation Dynamics*; Reisler, H., Noble, M., Wittig, C., Ashfold, M. N. R., Baggot, J. E., Eds.; Royal Society of Chemistry: London, 1987; p 162.
(6) Brühlmann, U.; Dubs, M.; Huber, J. R. *J. Chem. Phys.* **1987**, *86*, 1249.
(7) McCoustra, M. R. S.; Hippler, M.; Pfab, J. *Chem. Phys. Lett.* **1992**, *200*, 451.
(8) Schwartz-Lavi, D.; Rosenwaks, S. *J. Chem. Phys.* **1988**, *88*, 6922.
(9) Nonella, M.; Huber, J. R.; Untch, A.; Schinke, R. *J. Chem. Phys.* **1993**, *99*, 9553.
(10) Felder, P.; Keller, B. A.; Huber, J. R. *At., Mol. Clusters* **1987**, *6*, 185.
(11) Finke, H.; Spiecker, H.; Andersen, P. *J. Chem. Phys.* **1999**, *110*, 4777.
(12) Lav, R.; Schwartz-Lavi, D.; Bar, I.; Rosenwaks, S. *J. Phys. Chem.* **1987**, *91*, 5398.
(13) Schwartz-Lavi, D.; Bar, I.; Rosenwaks, S. *Chem. Phys. Lett*. **1986**, *128*, 123.
(14) August, J.; Brouard, M.; Docker, M. P.; Miline, C. J.; Simons, J. P.; Lavi, R.; Rosenwaks, S.; Schwartz-Lavi, D. *J. Phys. Chem.* **1987**, *91*, 5398.
(15) Simpson, C. J. M. S.; Griffiths, P. T.; Towrie, M. *Chem. Phys. Lett.* **1995**, *234*, 203.
(16) Simpson, C. J. M. S.; Griffiths, P. T.; Wallaart, H. L.; Towrie, M. *Chem. Phys. Lett*. **1996**, *263*, 19.
(17) Griffiths, P. T.; Simpson, C. J. M. S.; Stolte, C.; Towrie, M. *Chem. Phys. Lett*. **1999**, *315*, 158.
(18) Jenniskens, H. G.; Essenberg, W. V.; Kadodwala, M.; Kleyn, A. W. *Chem. Phys. Lett.* **1997**, *268*, 7.
(19) Jenniskens, H. G.; Philippe, L.; Essenberg, W. V.; Kadodwala, M.; Kleyn, A. W. *J. Chem. Phys*. **1998**, *108*, 1688.
(20) Jenniskens, H. G.; Essenberg, W. V.; Kadodwala, M.; Kleyn, A. W. *Surf. Sci.* **1998**, *402*, 140.
(21) Jenniskens, H. G.; Philippe, L.; Essenberg, W. V.; Kadodwala, M.; Kleyn, A. W. *J. Phys. Chem. B* **1988**, *102*, 8736.
(22) Fieberg, J. E.; White, J. M. *Chem. Phys. Lett.* **1999**, *306*, 103.
(23) Kim, C.; Zhao, W.; White, J. M. *Surf. Sci.* **2000**, *464*, 240.
(24) Zhao, W.; Kim, C.; White, J. M. *Surf. Sci.* **2000**, *451*, 267.
(25) Zhao, W.; Kim, C.; White, J. M. *J. Phys. Chem. A* **2001**, *105*, 2234.
(26) Lee, I.; Kim, S. K.; Zhao, W.; White, J. M. *Surf. Sci.* **2002**, *499*, 41.
(27) Lee, I.; Kim, S. K.; Zhao, W.; White, J. M. *Surf. Sci.* **2002**, *499*, 53.
(28) Kim, S. K.; White, J. M.; Agrawal, P. M.; Thompson, D. L. *J. Chem. Phys.* **2001**, *115*, 7657.
(29) Sremaniak, L. S.; Whitten, J. L. *Surf. Sci.* **2002**, *516*, 254.